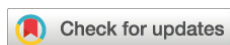


RESEARCH ARTICLE

Corrosion of austenitic Fe-Ni based alloys with various chromium and aluminum additions in a carburizing-oxidizing atmosphere at 800°C

Shu Liu¹ Yong Zhu¹ JunJie Cao^{1*}¹ Industrial Training Centre, Shenzhen Polytechnic University, Shenzhen 518000, China

Correspondence to: JunJie Cao, Industrial Training Centre, Shenzhen Polytechnic University, Shenzhen 518000, China; Email: cjj568288658@163.com

Received: February 3, 2024;

Accepted: April 13, 2024;

Published: April 17, 2024.

Citation: Liu S, Zhu Y and Cao J. Corrosion of austenitic Fe-Ni based alloys with various chromium and aluminum additions in a carburizing-oxidizing atmosphere at 800°C. *Mater Eng Res*, 2024, 6(1): 313-322. <https://doi.org/10.25082/MER.2024.01.002>

Copyright: © 2024 Shu Liu *et al.* This is an open access article distributed under the terms of the [Creative Commons Attribution-Noncommercial 4.0 International License](https://creativecommons.org/licenses/by-nc/4.0/), which permits all noncommercial use, distribution, and reproduction in any medium, provided the original author and source are credited.



Abstract: The corrosion behaviors of Fe-19Ni-13/21Cr-xAl ($x = 0, 2, 6$ at. %) alloys in a carburizing-oxidizing atmosphere were compared with those in a purely carburizing atmosphere at 800°C. For alloys with 13 at. % Cr, 2 at. % addition of Al did not improve the corrosion resistance effectively but induced a slightly increase of the total mass gain. 6 at. % addition of Al produced a large decrease of the total mass gain, therefore the corrosion resistance was improved significantly. For alloys with 21 at. % Cr, additions of Al did not affect the total mass gain obviously. Fe-19Ni-21Cr-xAl ($x = 0, 2, 6$ at. %) showed similar mass gain. Increase of Cr content from 13 at. % to 21 at. % is effective for protecting the alloys from the carbon attack for Al-free alloys and alloys with 2 at. % Al. However, addition of Cr is not so helpful for alloys with 6 at. % Al. The addition of oxygen improved the corrosion resistance of all alloys significantly except the Fe-19Ni-13Cr-6Al. Pure external chromia scales on alloys without Al and with 2 at. % Al could not suppress the inward diffusion of the carbon atoms. Aluminum and chromium worked together to form mixed oxide scales inhibiting the carbon attack totally on alloys with 6 at. % Al.

Keywords: carburization, Fe-Ni-Cr-Al, alumina, chromia, oxidation

1 Introduction

Austenitic Fe-Ni-Cr alloys are widely used in petrochemical industries as heat-resistant materials. Carburization and metal dusting, the mechanisms of which have been widely investigated [1], are two types of corrosion always occurring on these alloys used in atmospheres with high carbon activities. When the alloys were exposed to the gas mixtures with carbon activities (a_C) less than 1, carburization often occurs and the mechanical properties of the alloys will be reduced due to the formation of the internal carbides. While the metal dusting which is catastrophic always occurs when the alloys were exposed to gas mixtures with carbon activities larger than 1, the surface layers of the alloys are converted into mixtures of carbides, carbon coke and metal particles.

Many papers investigated the role of Cr_2O_3 , which is useful for protecting the alloys in oxidizing atmosphere [2, 3], on preventing the carbon attack in aggressive atmospheres. The Cr_2O_3 scales could not protect the substrate very well due to their evaporation and the formation of the chromium carbides. However, alumina could offer a much better protection than chromia in many aggressive environments with high carbon activities [4]. The critical Al content needed to form a protective alumina scale in gas mixtures with high carbon activities has been widely investigated [5–7]. But addition of Al to the austenitic alloys could promote the formation of ferrite which is bad for the mechanical properties of the alloys [4]. Therefore, investigation on how to promote the formation of external Al_2O_3 with less Al addition is significant. In many environments, more Cr content could result in smaller critical Al content to form a protective scale. However, the synergic effect between chromium and aluminum on the prevention of the carbon attack to the alloys in gas mixtures with high carbon activities has not been examined so far.

The aim of this paper is to investigate the corrosion behaviors of austenitic Fe-Ni based alloys with various Cr and Al additions in a carburizing-oxidizing atmosphere. The role of chromium on corrosion resistance of the alloys will be discussed in this paper, as well as the role of aluminum. Moreover, the interaction of chromium and aluminum and the role of their

mixed oxides will also be explored. In addition, the corrosion behaviors of alloys exposed to this carburizing-oxidizing atmosphere (denoted as C-O) are compared to those exposed to a purely carburizing atmosphere (denoted as C) which provides the same carbon activity as the C-O atmosphere used here to explore the role of oxygen on prevention of the carbon attack.

2 Experimental procedures

Six alloys with nominal composition (all in at. %, if not specified otherwise) Fe-19Ni-13/21Cr-xAl ($x = 0, 2, 6$) were prepared by vacuum induction melting using mixtures of high purity metals (wt. %) (99.9Fe, 99.0Cr, 99.9Ni, 99.7Al) and then cast in cylinders of 5 cm diameter, 10 cm high. The alloy ingots were subsequently annealed in 1 atm argon at 1000°C for 36 h to release the residual stresses and achieve a better equilibration. Their actual composition, measured by ICP spectrometry analysis, is shown in Table 1. According to the ternary phase diagram of Fe-20Ni-Cr (mass %) and the corresponding micrographs of the structure of the alloys which have been reported elsewhere [8]. The alloy Fe-19Ni-21Cr-6Al is composed of a mixture of a γ -phase matrix with Cr-rich γ' precipitates evenly distributed. Other alloys are all single γ -phase fcc. Samples were cut into $10 \times 8 \times 1.5$ mm from the ingots using a line saw and a 1 mm hole was drilled near one edge. All samples were mechanically abraded on successively finer abrasive papers down to 2000 grit and finally cleaned with water, acetone and ethanol and dried immediately before each test. The experiments were carried out at 800°C under 1 atm in a gas mixture of (vol.%) 21CH₄-15CO₂-64H₂ for 18 h in a microbalance Setaram B-92 using a Pt catalyst. The gases were premixed and dried by P₂O₅ before entering in the reaction chamber. Moreover, six alloys were also corroded in a gas mixture of (vol.%) 10CH₄-bal.H₂ which nominally contains only one oxidant carbon plus oxygen impurities, shown in Table 1, providing an oxygen pressure of about 10^{-29} atm. This oxygen pressure provided by the C atmosphere is sufficient to sustain the formation of Al₂O₃ rather than Cr₂O₃. The carbon activity provided by this C atmosphere is equal to 2.6, which is same as that produced by the C-O atmosphere used here. Therefore, the role of oxygen could be explored by comparing the corrosion behaviors of the same alloy exposed to the two different gas mixtures.

Table 1 Gas mixtures, calculated carbon activities and oxygen pressures for various exposure conditions

	CH ₄ (vol. %)	CO ₂ (vol. %)	H ₂ (vol. %)	aC	P _{O₂} (atm)	Impurities
C-O ¹	10	—	90	2.6	$\leq 10^{-29}$ *	O ₂ \leq 1.00 ppm CO \leq 0.18 ppm CO ₂ \leq 0.18 ppm H ₂ O \leq 2.90 ppm
C ²	21	15	64	2.6	10 ⁻²⁴ #	

Notes: ¹: the carburizing oxidizing atmosphere; ²: the purely carburizing atmosphere; *: the oxygen pressures are calculated according to the content of the impurities in the gas mixtures.

The carbon activity and the oxygen pressure of the C-O gas mixture used here is determined by the virtual equilibrium of the following reactions:



The corroded samples were examined by means of optical microscopy (OM), scanning electron microscopy (SEM), generally using the back-scattered electron image (BEI) mode, energy dispersive X-ray microanalysis (EDX), and XRD to study the structure of the scales, to identify the nature of the phases and their distribution and for elemental analysis. The reacted samples were etched with Murakami's etchant to reveal the precipitated carbides.

3 Results

3.1 Corrosion kinetics

The kinetic curves for all alloys exposed to the C-O atmosphere at 800°C for 18 h are shown in Figure 1a-1b as linear plots and Figure 1c-1d as parabolic plots, respectively. For Fe-19Ni-13Cr, a parabolic stage, lasting from 4 h to the end, appeared with a parabolic rate constant k_p equal to $6.35 \times 10^{-13} \text{ g}^2 \text{ cm}^{-4} \text{ s}^{-2}$ after the initial incubation period. For Fe-19Ni-13Cr-2Al, the k_p for

the parabolic stage, appeared after the initial stage, lasting from 1 h to 6.25 h is equal to $1.26 \times 10^{-12} \text{ g}^2 \text{ cm}^{-4} \text{ s}^{-2}$. After this, the parabolic rate constant decreased more rapidly with time than predicted by the parabolic rate law. The kinetic curve for Fe-19Ni-13Cr obeyed the similar law with Fe-19Ni-13Cr, a parabolic stage, lasting from 1 h to the end, appeared with a parabolic rate constant k_p equal to $1.56 \times 10^{-14} \text{ g}^2 \text{ cm}^{-4} \text{ s}^{-2}$ after the initial period. The parabolic rate constant k_p equal to $4.4 \times 10^{-14} \text{ g}^2 \text{ cm}^{-4} \text{ s}^{-2}$ for Fe-19Ni-21Cr. Fe-19Ni-21Cr-2Al corroded in the C-O atmosphere produced an initial stage of about 1 h, followed by a nearly parabolic stage with $k_p = 1.4 \times 10^{-14} \text{ g}^2 \text{ cm}^{-4} \text{ s}^{-2}$ lasting to the end. A similar kinetic behavior produced by Fe-19Ni-21Cr-6Al, with a parabolic stage with $k_p = 2.2 \times 10^{-14} \text{ g}^2 \text{ cm}^{-4} \text{ s}^{-2}$ lasting from 2.2 h to the end.

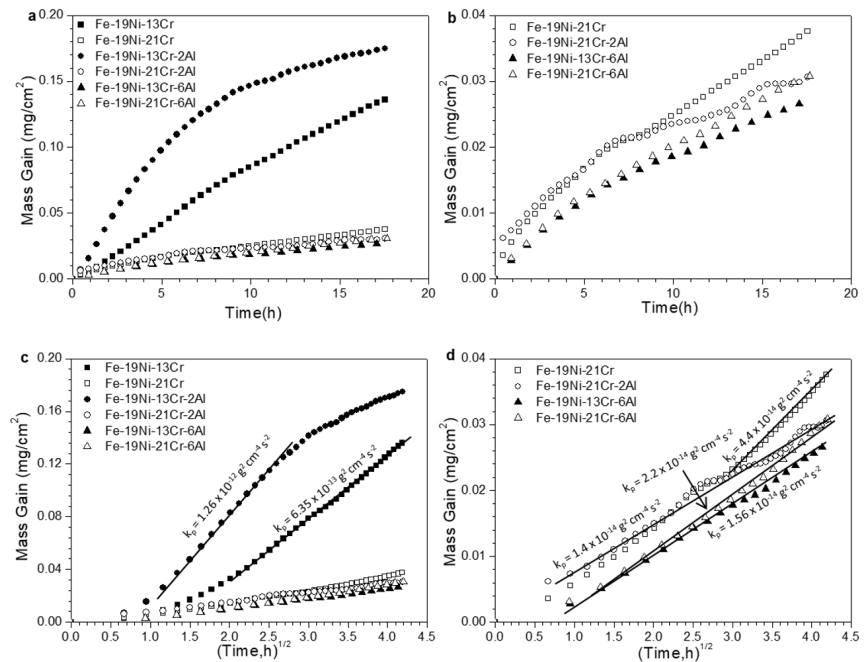


Figure 1 Kinetic curves for the corrosion of Fe-19Ni-13/21Cr-xAl ($x = 0, 2, 6$ at.%) in $0.21\text{CH}_4\text{-}0.15\text{CO}_2\text{-}0.64\text{H}_2$ at 800°C for 18h. (a): linear plots; (b): enlarged view of linear plot; (c): parabolic plots; (d): enlarged view of parabolic plot.

For alloys with 13 at. % Cr, small addition of Al (2 at. %) did not improve the corrosion resistance effectively but induced a slightly increase of the total mass gain. 6 at. % addition of Al produced a large decrease of the total mass gain and the parabolic rate constant, therefore the corrosion resistance was improved significantly. For alloys with 21 at. % Cr, additions of Al did not affect the total mass gain obviously. Fe-19Ni-21Cr, Fe-19Ni-21Cr-2Al and Fe-19Ni-21Cr-6Al showed similar mass gain.

Increase of Cr content from 13 at. % to 21 at. % is effective for protecting the alloys from the carbon attack for Al-free alloys and alloys with 2 at. % Al. However, addition of Cr is not so helpful for alloys with 6 at. % Al.

The role of oxygen could be explored by comparing the kinetic curves of the same alloy exposed to the C-O atmosphere used here and the C atmosphere with the same carbon activity, shown in Figure 2. According to the figures, addition of oxygen to the gas mixture decreased the total mass gains largely and had a strong beneficial effect on the improvement of the corrosion resistance of all alloys except Fe-19Ni-13Cr-6Al.

3.2 Morphology and structure of the scales

The morphology of the cross-sections for all alloys exposed to the C-O atmosphere used here are shown in Figure 3 to Figure 8. According to Figure 3, intragranular carbides unevenly distributed in Fe-19Ni-13Cr. Intergranular carbides also formed in this alloy and an external layer of Cr_2O_3 appeared. Similarly, internal carbides appeared in Fe-19Ni-13Cr-2Al (Figure 4). The whole surface of the alloy was covered by a thin Cr_2O_3 layer and internal oxides Al_2O_3 formed in the subsurface zone. No internal carbides appeared in Fe-19Ni-13Cr-6Al exposed to the C-O atmosphere (Figure 5). An external oxide layer rich in Cr and Al protected the substrate from the carbon attack. Internal oxides Al_2O_3 still formed in the subsurface zone.

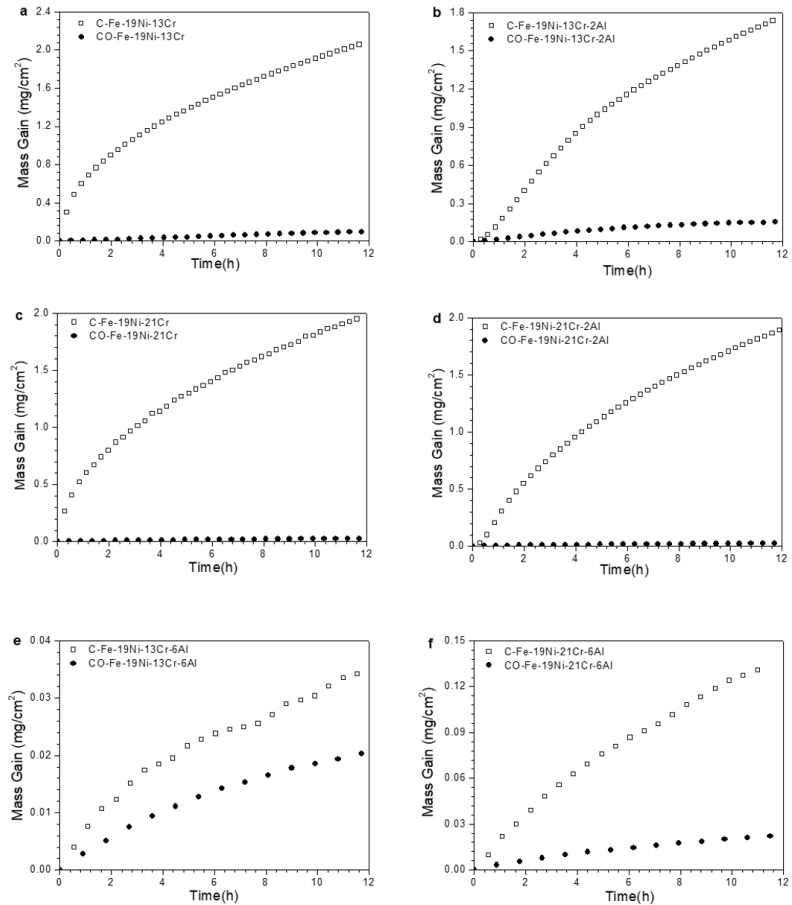


Figure 2 Kinetic curves for the corrosion of Fe-19Ni-13/21Cr-xAl ($x = 0, 2, 6$ at.%) in $10\%CH_4/H_2$ and $0.21CH_4-0.15CO_2-0.64H_2$ at $800^\circ C$ for 12h. (a): Fe-19Ni-13Cr; (b): Fe-19Ni-13Cr-2Al; (c): Fe-19Ni-21Cr; (d): Fe-19Ni-21Cr-2Al; (e): Fe-19Ni-13Cr-6Al; (f): Fe-19Ni-21Cr-6Al.

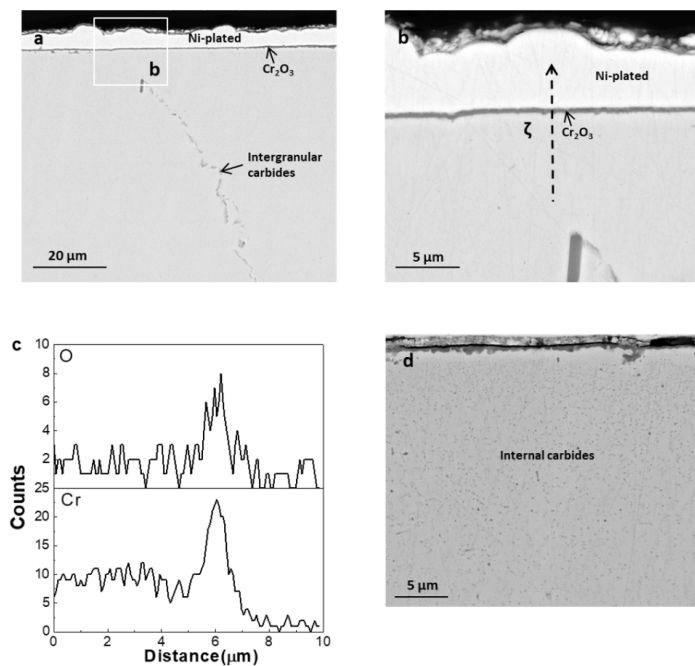


Figure 3 Micrograph of cross section of Fe-19Ni-13Cr reacted in $0.21CH_4-0.15CO_2-0.64H_2$ at $800^\circ C$ for 18h (SEM/BEI) (a) general view; (b) enlarged view of the outer region of (a); (c) elements distribution of line ζ in (b); (d) general view.

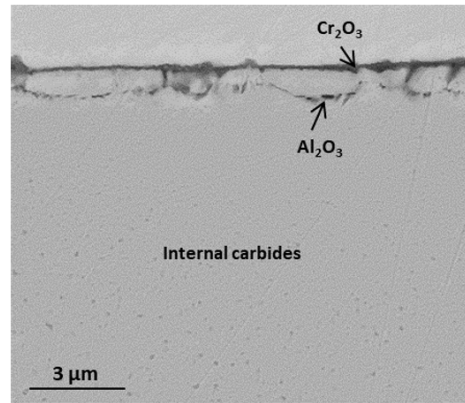


Figure 4 Micrograph of cross section of Fe-19Ni-13Cr-2Al reacted in $0.21\text{CH}_4\text{-}0.15\text{CO}_2\text{-}0.64\text{H}_2$ at 800°C for 18h (SEM/BEI)

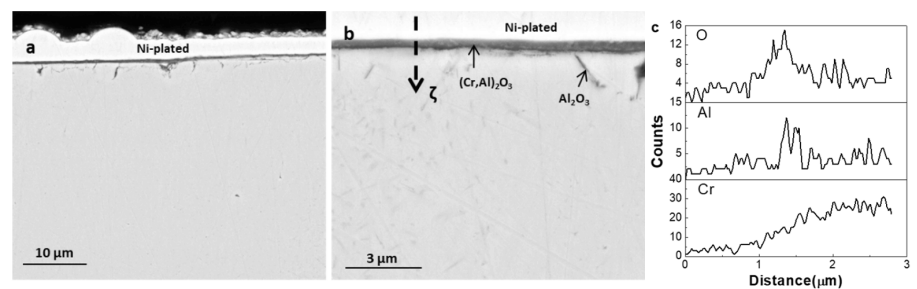


Figure 5 Micrograph of cross section of Fe-19Ni-13Cr-6Al reacted in $0.21\text{CH}_4\text{-}0.15\text{CO}_2\text{-}0.64\text{H}_2$ at 800°C for 18h (SEM/BEI) (a)general view; (b) enlarged view of the outer region; (c) elements distribution of line ζ in (b).

An external Cr_2O_3 layer covered the whole surface of Fe-19Ni-21Cr (Figure 6). Carbides developed into the substrate along the grain boundaries with a few carbides spread in the grains near the boundaries. According to Figure 7, intragranular carbides unevenly distributed in Fe-19Ni-21Cr-2Al. A layer of Cr_2O_3 formed on this alloy with internal Al_2O_3 appeared in the subsurface zone. Many internal Al_2O_3 particles grew along the grain boundaries followed by intergranular carbides particles which spread deep into the substrate. An external oxide layer rich in Cr and Al, which could resist the carbon attack effectively, formed on Fe-19Ni-21Cr-6Al, no carbides appeared in the substrate. (Figure 8)

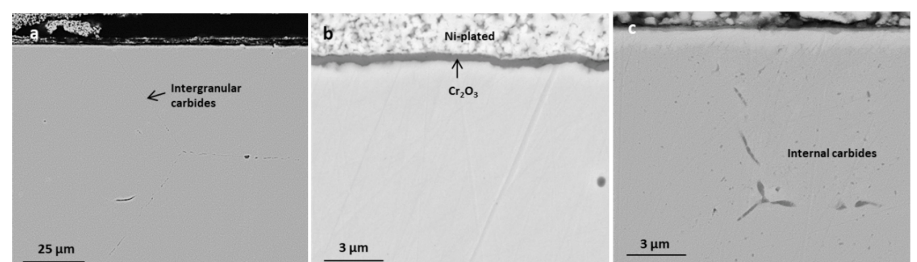


Figure 6 Micrograph of cross section of Fe-19Ni-21Cr reacted in $0.21\text{CH}_4\text{-}0.15\text{CO}_2\text{-}0.64\text{H}_2$ at 800°C for 18h (SEM/BEI) (a)general view; (b) enlarged view of the outer region; (c) enlarged view of the inner region.

According to the morphology of the cross-sections of all alloys, 2 at. % addition of Al could not affect the corrosion resistance, but 6 at. % Al addition could improve the resistance to the carbon attack significantly. By comparing with the morphology of the cross-sections for all alloys exposed to the C atmosphere which was described elsewhere [8], the number and the volume of the internal carbides in all alloys exposed to the C-O atmosphere for 18 h are significantly smaller than those in the same alloy exposed to the C atmosphere with the same carbon activity for 12 h except Fe-19Ni-13Cr-6Al in which no internal carbide appeared in the C atmosphere. Therefore, addition of oxygen could promote the formation of external oxides which could protect the substrate from the carbon attack effectively.

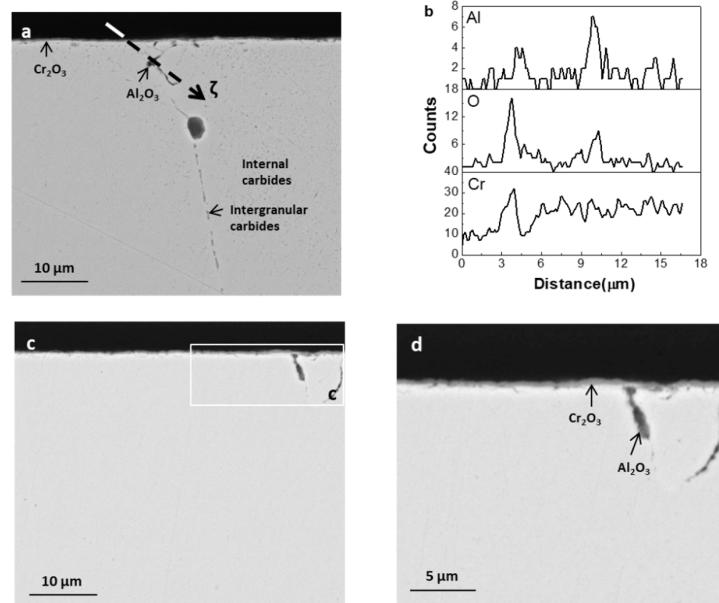


Figure 7 Micrograph of cross section of Fe-19Ni-21Cr-2Al reacted in 0.21CH₄-0.15CO₂-0.64H₂ at 800°C for 18h (SEM/BEI) (a) general view; (b) elements distribution of line ζ in (a); (c) general view; (d)enlarged view of the outer region of (c).

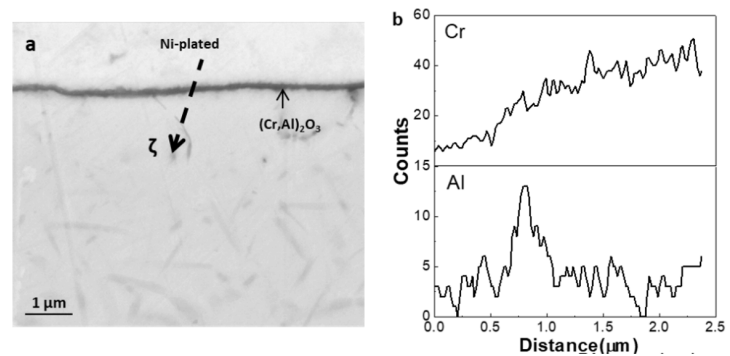


Figure 8 Micrograph of cross section of Fe-19Ni-21Cr-6Al reacted in 0.21CH₄-0.15CO₂-0.64H₂ at 800°C for 18 h (SEM/BEI) (a) general view; (b) elements distribution of line ζ in (a).

4 Discussion

The carbon activity in carburizing atmosphere composed of mixtures of CH₄ and H₂ can be calculated from the condition of equilibrium of reaction (1). If carbon is present in its stable state (graphite), its activity is equal to unity. In this case, the equilibrium constant K_1 takes the form:

$$K_1 = \frac{P(\text{H}_2)_{(\text{eq})}^2}{P(\text{CH}_4)_{(\text{eq})}} \quad (4)$$

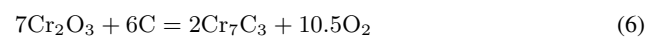
This equilibrium involving graphite is only possible if the partial pressures of H₂ and CH₄ satisfy Eq. (3) with the correct value of K_1 for the temperature considered. When dealing with practical problems in which Eq. (3) is generally not fulfilled, many researchers rewrite K_1 in the form:

$$K_1 = a_c \frac{P(\text{H}_2)^2}{P(\text{CH}_4)} \quad (5)$$

where $P(\text{H}_2)$ and $P(\text{CH}_4)$ are the actual partial pressures of the two gas species in the practical gas mixture, while a_c is the so-called virtual carbon activity and can be calculated by introducing the values of K_1 , $P(\text{H}_2)$ and $P(\text{CH}_4)$ into Eq. (4). The carbon activities calculated in this way are used to show the degree of deviation from equilibrium of reaction (1). In particular, a_c values < 1 show that reaction (1) should go proceed to the left so that carbon would not be

deposited and, if present, should be consumed. Conversely, when $a_C > 1$ reaction (1) should go to the right, resulting in the decomposition of CH_4 with deposition of solid carbon. In general, the virtual carbon activity can be used to predict the actual direction of reaction (1) and to describe the degree of deviation from equilibrium in a quantitative way. When $a_C > 1$, the higher is its value, the greater is the driving force for the carbon deposition and the more likely the probability of metal dusting.

According to HSC version 6.0 [9], the dissociation pressure of Cr_2O_3 , $P_{\text{Cr}_2\text{O}_3/\text{alloy}}$, could be calculated as $P_{\text{Cr}_2\text{O}_3/\text{alloy}} = 9.125 \times 10^{-28}$ atm for alloys with 13 at. % Cr and $P_{\text{Cr}_2\text{O}_3/\text{alloy}} = 5.775 \times 10^{-28}$ atm for alloys with 21 at. % Cr, using activity coefficients for Cr at 850°C here as approximate values at 800°C [10]. The two values are smaller than the equilibrium oxygen pressure provided by the C-O atmosphere used here (3.94×10^{-24} atm). However, according to HSC version 6.0, assuming the activity coefficient for iron equal to 1, the dissociation pressure of FeO, $P_{\text{FeO}/\text{alloy}}$, could be calculated as 2.65×10^{-19} atm for alloys with 13 at. % Cr and 3.4×10^{-19} atm for alloys with 21 at. % Cr. The two values are higher than the equilibrium oxygen pressure provided here. Therefore, oxygen could react with chromium instead of iron. However, chromia could also react with carbon on the surface of the present alloys according to the following reaction:



Although Cr_3C_2 appeared in many alloys exposed to gas mixtures containing high carbon activities, the carbide M_7C_3 rich in Fe could equilibrate with graphite directly [11]. Thus, Cr_3C_2 is neglected. According to the above reaction, chromia is more stable than Cr_7C_3 on the surface of the present alloys, considering the equilibrium oxygen pressure and the carbon activity of this gas mixture. This prediction agrees with the experimental results, chromia or mixed oxide rich in Cr formed externally on all alloys instead of the carbides.

According to Grabke [12], the solubility of carbon in chromia and alumina at 1000°C is below 0.01 ppm. Therefore, carbon atoms could not be able to permeate efficiently through dense external chromia and alumina scales. Theoretically, formation of continuous and compact external chromia or alumina or their mixed oxide scales could protect the substrate from the carbon attack effectively. To clarify this problem, it is useful to calculate the critical content of Cr and Al needed to form continuous and protective scales on this type of Fe-Ni-Cr-Al alloys in the absence of carbon.

According to Wagner [13, 14], for binary A-B alloys, A is the most-noble component and B is the most-reactive component, exposed to a purely oxidizing gas mixture with oxygen pressure insufficient to form the oxide of A, the critical mole fraction of B, needed for the transition from the internal to the external oxidation, is given by

$$N_B^* = f_v^* F(h) \frac{V(\text{all})}{V(\text{BO}_v)} \quad (7)$$

Where N_B^* is the critical content of B, BO_v is the formula of the oxide of B, f_v^* is the critical value of the volume fraction of BO_v in the internal oxidation zone, f_v^* , corresponding to a B content equal to N_B^* , while $V(\text{all})$ and $V(\text{BO}_v)$ are the molar volumes of the alloy and of BO_v (per mole of metal). Moreover, h is equal to $\gamma\varphi^{1/2}$, where γ is the kinetic parameter appearing in the equation

$$\xi^2 = 4\gamma^2 D_o t \quad (8)$$

where ξ is the thickness of the internal-oxidation zone at time t and D_O is the diffusion coefficient of oxygen in A and φ is equal to D_O/D_B , where D_B is the diffusion coefficient of B in A. In particular, the critical value of f_v, f_v^* , has been found equal to 0.3 for the oxidation of Ag-In alloys, a value which has then been used frequently [15]. The equation needed for the calculation of the kinetic parameter γ of internal oxidation has the form [16]

$$\frac{N_0^s}{vN_B^o} = \frac{G(\gamma)}{F(h_B)} \quad (9)$$

where $G(r)$ [13] and $F(r)$ [13] are two auxiliary functions defined as

$$G(r) = \pi^{1/2} r \exp(r^2) \text{erf}(r) \quad (10)$$

$$F(r) = \pi^{1/2} r \exp(r^2) [1 - \text{erf}(r)] \quad (11)$$

The contents of Al are so low that the four quaternary Fe-Ni-Cr-Al alloys, used to calculate the critical Cr content, were simplified into ternary Fe-Ni-Cr alloys. Applying Wagner's theory into

this investigation, A, the most-noble component, represents the Fe-Ni matrix and B represents chromium. The diffusion coefficient of oxygen in γ -Fe, D_o , is equal to $3.37 \times 10^{-8} \text{ cm}^2/\text{s}$ at 800°C and the diffusion coefficient of chromium (D_B) is equal to $4.8 \times 10^{-12} \text{ cm}^2/\text{s}$ at the same temperature [17]. Moreover, the solubility of oxygen in γ -Fe follows the following equation [17]:

$$\frac{N_{\text{O}}^s}{p_{\text{O}_2}^{1/2}} = \exp\left(-\frac{-175100 + 98.8T}{RT}\right) \quad (12)$$

Submitting the oxygen pressure and the test temperature into the above equation, the solubility of oxygen (N_{O}^s) in γ -Fe at 800°C is equal to 1.83×10^{-10} . The three values are used here as an approximation. v is the O/B ratio in BO_v which is equal to 1.5 in the case of Cr_2O_3 . Introduction of the D_o , D_{Cr} and N_{O}^s into equations (7) and (9) yields $N_{Cr}^* = 2.38 \times 10^{-5}$. Similarly, the critical content of Al required from the transition for the internal to the external formation of Al_2O_3 in a purely oxidizing atmosphere with the same oxygen pressure as the gas mixture used here could also be calculated. The diffusion coefficient of aluminum in γ -Fe at 800°C is equal to $1.9 \times 10^{-10} \text{ cm}^2/\text{s}$ [17], a value used here as approximation. Introduction of the D_o , D_{Al} and N_{O}^s into equations (7) and (9) yields $N_{AL}^* = 1.16 \times 10^{-6}$.

The calculated chromium content and aluminum content are much smaller than those presented in alloys used here. Therefore, all alloys here could develop continuous scales in purely oxidizing atmosphere with similar oxygen pressure. The predictions appear to be in good agreement with the experimental results, continuous scales formed on all alloys, although the samples were exposed to gas mixtures containing not only oxygen but also carbon. The continuous oxide scales actual play an important role in prohibiting carbon attack. The total weight gains for alloys exposed to the C atmosphere were larger than those for alloys exposed to the C-O atmosphere used here. This effect was more obvious for Al-free alloys and the alloys with 2 at. % Al. By comparing the morphology of the cross-sections, all alloys sustain serious carbon attack in C atmosphere except the Fe-19Ni-13Cr-6Al on which a continuous alumina scale appeared [8].

However, although continuous chromia scales formed an Al-free alloys and alloys presenting 2 at. % Al, internal carbides still appeared, indicating weaker protection provided by the external chromia than alumina and the internal alumina could not protect the substrate very well which were observed constantly elsewhere [18, 19]. According to Grabke [12], carbon atoms could not penetrate through chromia and alumina grains effectively. However, different from alumina, carbon could diffuse inwards through chromia scales via oxide grain boundaries [20–22]. In this study, internal carbides formed in Al-free alloys and alloys with 2 at. % Al which were covered by continuous chromia. Therefore, continuous chromia scales formed here could not suppress carbon attack totally. Carbon containing species could diffuse inwards via grain boundaries in chromia scales.

For Fe-19Ni-13Cr-6Al and Fe-19Ni-21Cr-6Al, due to their high Al contents, large amount of alumina particles formed on the surfaces of the alloys as well as chromia. The oxide particles grow laterally and connect with each other. External mixed oxide scale rich in Cr and Al show better performance than chromia scale in hindering carbon-containing species diffuse inwards.

5 Conclusion

The corrosion behaviors of the alloys Fe-19Ni-13/21Cr-xAl ($x = 0, 2, 6$ at. % Al) exposed to a gas mixture (vol.%) $21\text{CH}_4-15\text{CO}_2-64\text{H}_2$, providing a carbon activity $a_C = 2.6$ and an oxygen pressure $P_{\text{O}_2} = 3.94 \times 10^{-24} \text{ atm}$, were studied. Continuous chromia scales, formed on Fe-19Ni-13/21Cr-xAl ($x = 0, 2$ at. % Al), were not so protective due to the carbon containing species diffused inwards through grain boundaries in the scales. Mixed scales rich in Cr and Al formed on Fe-19Ni-13/21Cr-6Al were effective. External chromia and alumina worked together to hinder the carbon attack. Corrosion behaviors were compared with those exposed to a purely carburizing mixture providing the same carbon activity. The addition of oxygen improved the corrosion resistance of the alloys effectively due to the formation of external oxide scales, except Fe-19Ni-13Cr-6Al protected very well by the external alumina scale formed in the purely carburizing atmosphere with oxygen produced by the impurities.

Acknowledgements

This work was financially supported by NSFC (Grant No. 51801026 and 51671203), the Foundation for Young Talents of Shenzhen Polytechnic (Grant No. 601822K35018), Foundation

for Young Talents in Higher Education of Guangdong (Grant No. 601821K35055).

Conflicts of interest

The authors declare that they have no conflict of interest.

References

- [1] Rahmel A, Grabke HJ, Steinkusch W. Carburization - introductory survey. *Materials and Corrosion*. 1998, 49(4): 221-225.
[https://doi.org/10.1002/\(SICI\)1521-4176\(199804\)49:4<221::AID-MACO221>3.0.CO;2-X](https://doi.org/10.1002/(SICI)1521-4176(199804)49:4<221::AID-MACO221>3.0.CO;2-X)
- [2] Gheno T, Monceau D, Zhang J, et al. Carburisation of ferritic Fe–Cr alloys by low carbon activity gases. *Corrosion Science*. 2011, 53(9): 2767-2777.
<https://doi.org/10.1016/j.corsci.2011.05.013>
- [3] Salas O, Melo-Máximo DV, Oseguera J, et al. Role of PVD oxide coatings on HK40 cast steel during short and long exposure to C-rich atmospheres. *Materials Characterization*. 2013, 83: 58-67.
<https://doi.org/10.1016/j.matchar.2013.05.016>
- [4] Yamamoto Y, Brady MP, Lu ZP, et al. Creep-Resistant, Al₂O₃-Forming Austenitic Stainless Steels. *Science*. 2007, 316(5823): 433-436.
<https://doi.org/10.1126/science.1137711>
- [5] Mitchell DRG, Young DJ. The effect of molybdenum and aluminium additions on the carburization behaviour of high temperature steel. *Journal of Materials Science Letters*. 1993, 12(14): 1076-1079.
<https://doi.org/10.1007/bf00420526>
- [6] Becker P, Young DJ. Carburization resistance of nickel-base, heat-resisting alloys. *Oxidation of Metals*. 2007, 67(5-6): 267-277.
<https://doi.org/10.1007/s11085-007-9058-x>
- [7] Allam IM. Carburization/Oxidation Behavior of Alloy Haynes-214 in Methane–Hydrogen Gas Mixtures. *Oxidation of Metals*. 2009, 72(3-4): 127-144.
<https://doi.org/10.1007/s11085-009-9151-4>
- [8] Liu S, Cui J. Carburization effect of Austenitic alloys with various Cr and Al additions under the methane/hydrogen atmosphere on the corrosion behaviors of steels. *Materials Engineering Research*. 2021, 3(1): 165-174.
<https://doi.org/10.25082/mer.2021.01.005>
- [9] Roine A. HSA Chemistry Version 6.0, Outokumpu Research, Oy, Finland, 2006.
- [10] Colwell JA, Rapp RA. Reactions of Fe–Cr and Ni–Cr alloys in CO/CO₂ gases at 850 and 950 °C. *Metallurgical Transactions A*. 1986, 17(6): 1065-1074.
<https://doi.org/10.1007/bf02661273>
- [11] Kinniard SP, Young DJ, Trimm DL. Effect of scale constitution on the carburization of heat resistant steels. *Oxidation of Metals*. 1986, 26(5-6): 417-430.
<https://doi.org/10.1007/bf00659345>
- [12] Wolf I, Grabke HJ, Schmidt P. Carbon transport through oxide scales on Fe–Cr alloys. *Oxidation of Metals*. 1988, 29(3-4): 289-306.
<https://doi.org/10.1007/bf00751801>
- [13] Wagner C. Reaktionstypen bei der Oxydation von Legierungen. *Zeitschrift für Elektrochemie, Berichte der Bunsengesellschaft für physikalische Chemie*. 1959, 63(7): 772-782.
<https://doi.org/10.1002/bbpc.19590630713>
- [14] Wagner C. Oxidation of Alloys Involving Noble Metals. *Journal of The Electrochemical Society*. 1956, 103(10): 571.
<https://doi.org/10.1149/1.2430159>
- [15] Rapp RA. The transition from internal to external oxidation and the formation of interruption bands in silver-indium alloys. *Acta Metallurgica*. 1961, 9(8): 730-741.
[https://doi.org/10.1016/0001-6160\(61\)90103-1](https://doi.org/10.1016/0001-6160(61)90103-1)
- [16] RAPP RA. Kinetics, Microstructures and Mechanism of Internal Oxidation - Its Effect and Prevention in High Temperature Alloy Oxidation. *Corrosion*. 1965, 21(12): 382-401.
<https://doi.org/10.5006/0010-9312-21.12.382>
- [17] Young J. Chapter 1 The Nature of High Temperature Oxidation. *High Temperature Oxidation and Corrosion of Metals*. Published online 2008: 1-27.
[https://doi.org/10.1016/s1875-9491\(08\)00001-x](https://doi.org/10.1016/s1875-9491(08)00001-x)
- [18] Zhang G, Huang YP, Jiang E, et al. Effect of aluminium addition on the oxidation and carburization behaviour of austenitic stainless in high-temperature SCO₂ environments. *Corrosion Science*. 2024, 226: 111666.
<https://doi.org/10.1016/j.corsci.2023.111666>
- [19] Liu S, Guo XH, Cui J, et al. Corrosion Behavior of Fe-Base Austenitic Alloys with Various Al Additions in a Carburizing–Oxidizing Mixture at 900 °C. *Oxidation of Metals*. 2020, 94(1-2): 165-177.
<https://doi.org/10.1007/s11085-020-09985-4>

- [20] Olivares RI, Young DJ, Nguyen TD, et al. Resistance of High-Nickel, Heat-Resisting Alloys to Air and to Supercritical CO₂ at High Temperatures. *Oxidation of Metals*. 2018, 90(1-2): 1-25.
<https://doi.org/10.1007/s11085-017-9820-7>
- [21] Nguyen TD, La Fontaine A, Yang L, et al. Atom probe study of impurity segregation at grain boundaries in chromia scales grown in CO₂ gas. *Corrosion Science*. 2018, 132: 125-135.
<https://doi.org/10.1016/j.corsci.2017.12.024>
- [22] Young DJ, Zhang J. Alloy Corrosion by Hot CO₂ Gases. *JOM*. 2018, 70(8): 1493-1501.
<https://doi.org/10.1007/s11837-018-2944-7>